ehp ENVIRONMENTAL HEALTH PERSPECTIVES
http://www.ehponline.org

Combined Effects of High-Dose Bisphenol A and Oxidizing Agent ($KBrO_3$) on Cellular Microenvironment, Gene Expression, and Chromatin Structure of Ku70-deficient Mouse Embryonic Fibroblasts

Natalie R. Gassman, Erdem Coskun, Pawel Jaruga, Miral Dizdaroglu, and Samuel H. Wilson

http://dx.doi.org/10.1289/EHP237

Received: 27 July 2015
Revised: 26 October 2015
Accepted: 28 March 2016
Published: 15 April 2016

Environ Health Perspect DOI: 10.1289/EHP237
Advance Publication: Not Copyedited

Combined Effects of High-Dose Bisphenol A and Oxidizing Agent ($KBrO_3$) on Cellular Microenvironment, Gene Expression, and Chromatin Structure of Ku70-deficient Mouse Embryonic Fibroblasts

Natalie R. Gassman[1†], Erdem Coskun[2,3], Pawel Jaruga[2], Miral Dizdaroglu[2], and Samuel H. Wilson[1]

[1]Genome Integrity and Structural Biology Laboratory, NIEHS, National Institutes of Health, Research Triangle Park, North Carolina, USA; [2]Biomolecular Measurement Division, National Institute of Standards and Technology, Gaithersburg, Maryland, USA; [3]Faculty of Pharmacy, Gazi University, Ankara, Turkey. †Current address: Department of Oncologic Sciences, University of South Alabama Mitchell Cancer Institute, Mobile, Alabama USA

Address correspondence to Samuel H. Wilson, Genome Integrity and Structural Biology Laboratory, National Institute of Environmental Health Sciences, National Institutes of Health, P.O. Box 12233, Research Triangle Park, NC 27709-12233 USA. Telephone: 919-541-4701. Fax: 919-541-4724. E-mail: wilson5@niehs.nih.gov

Short title: High-dose BPA alters cellular microenvironment

Acknowledgments: We thank the NIEHS Microarray Core (Dr. Kevin Gerrish, Joetta Hitchcock-Smith, and Liwen Liu) and Dr. Carl Bortner and Maria Sifre for their assistance with flow cytometry measurements. This research was supported by Research Project Numbers Z01-ES050158 and Z01-ES050159 in the Intramural Research Program of the National Institutes of Health, National Institute of Environmental Health Sciences. NRG is funded by 1K99ES023813-

01. The funders had no role in study design, data collection and analysis, decision to publish, or preparation of the manuscript. Certain commercial equipment or materials are identified in this paper in order to specify adequately the experimental procedure. Such identification does not imply recommendation or endorsement by the National Institute of Standards and Technology, nor does it imply that the materials or equipment identified are necessarily the best available for the purpose.

Competing financial interests: The authors declare they have no actual or potential competing financial interests.

Abstract

Background: Exposure to bisphenol A (BPA) has been reported to alter global gene expression, induce epigenetic modifications, and interfere with complex regulatory networks of cells. In addition to these reprogramming events, we have demonstrated that BPA exposure generates reactive oxygen species and promotes cellular survival when co-exposed with the oxidizing agent potassium bromate ($KBrO_3$).

Objectives: To determine the cellular microenvironment changes induced by co-exposure of BPA and $KBrO_3$ versus either agent alone.

Methods: Ku70-deficient cells were exposed to 150 μM BPA, 20 mM $KBrO_3$, or co-exposed with both agents. 4 and 24 h post-damage initiation by $KBrO_3$, with BPA only samples timed to coincide with these designated time points, we performed whole genome microarray analysis and evaluated chromatin structure, DNA lesion load, glutathione content, and intracellular pH.

Results: We found that 4 h post-damage initiation BPA exposure and co-exposure transiently condensed chromatin compared to untreated and $KBrO_3$ alone treated cells and reduced the transcription of DNA repair proteins. At this time point, BPA exposure and co-exposure also reduced the change intracellular pH observed after $KBrO_3$ alone. 24 h post-damage initiation, BPA exposed cells showed less condensed chromatin than $KBrO_3$ alone; the intracellular pH of the co-exposed treatment was reduced significantly compared to untreated and $KBrO_3$ treated cells; and significant up-regulation of DNA repair proteins was also observed after co-exposure.

Conclusion: These results support the induction of an adaptive response by BPA co-exposure that alters the microcellular environment and modulates DNA repair. Further work is required to determine whether BPA induces similar DNA lesions *in vivo* at environmentally relevant doses; however, in the Ku-deficient mouse embryonic fibroblasts, exposure to a high dose of BPA was associated with changes in the cellular microenvironment that may promote survival.

Introduction

World-wide production of bisphenol A (BPA) has increased exponentially as the demand for this chemical in consumer products, from food and beverage containers to epoxies, has grown (Vandenberg et al. 2007). This increase has resulted in elevated BPA levels in the air, water, soil, and also in human samples (Vandenberg et al. 2007; Vandenberg et al. 2010). The ubiquity of BPA in our environment has resulted in concurrent exposures of BPA with endogenous and exogenous DNA damaging events. Together these exposures can increase the damage load of genomic DNA and have implications for genomic stability and the development and progression of disease. While, the estrogenic properties of BPA are one source of concern, BPA exposure has been shown to cause DNA damage independent of its estrogenic properties over a range of doses from environmentally relevant nanomolar to high micromolar, in both *in vitro* and *in vivo* models (Iso et al. 2006; Nishimura et al. 2014; Tiwari et al. 2012; Wu et al. 2013; Yang et al. 2009). Yet, how the DNA damage response and repair pathways address BPA exposure has not been extensively investigated.

We previously demonstrated that exposure to high-dose BPA (150 μM) generates reactive oxygen species (ROS) in a model experimental system of Ku70-deficient mouse embryonic fibroblast (MEF) (Gassman et al. 2015). The Ku70-deficient cell line is sensitive to oxidizing agents, and its deficiency in double-strand break repair by non-homologous end joining, which also serves as a back-up repair pathway for the base excision repair (BER) pathway, provides a window into the cellular responses to oxidatively induced DNA damage (Choi et al. 2014; Li et al. 2013). Using this repair deficient cell line, high-dose BPA exposure was found to increase oxidatively induced DNA lesions in the genomic DNA (Gassman et al. 2015). Since these BPA-

induced DNA lesions would occur in concert with other DNA damaging events during environmental exposures, the effects of co-exposure of BPA with the dietary oxidizing agent, potassium bromate ($KBrO_3$) were also examined. $KBrO_3$, which is primarily used in flour or bread-making to improve elasticity and rising, induces ROS and oxidatively induced DNA lesions and has been shown to be a carcinogen at high doses in various animal models (Ballmaier and Epe 2006). Though it has been banned in a number of countries, it is still used in the US and co-exposure with BPA from food stuffs may occur, though this co-exposure would occur at lower doses than described here and in our previous work. We chose to examine the effects of a high dose of $KBrO_3$ over a short exposure period to concentrate the effects of this agent. Using these conditions, we found that co-exposure of both BPA and $KBrO_3$ resulted in a further increase in the levels of oxidatively induced DNA lesions (Table 1). Both thymine glycol and 2,6-diamino-4-hydroxy-5-formamidopyrimidine (FapyGua) levels are significantly elevated over control and over $KBrO_3$ alone (Gassman et al. 2015). Surprisingly, despite the fact that both BPA and $KBrO_3$ induce oxidative stress, an improvement in cellular survival was observed after co-exposure to both agents (Figure 1, adapted from Gassman et al. 2015).

Further examination of this cellular protective effect revealed that in the early repair window of 4 h post exposure, BPA co-exposure reduced DNA strand break signaling and resulted in the persistence of oxidatively induced DNA lesions (Table 1) (Gassman et al. 2015), beyond the typical DNA repair window of 2-4 h (Hollenbach et al. 1999; Jaruga and Dizdaroglu 1996). This combination of reduced strand break initiation coupled with increased lesion load is often observed in glycosylase-deficient cells, suggesting that BPA may prevent initiation of repair of oxidized base lesions, reducing the production of toxic strand break intermediates (Roth and

Samson 2002; Sobol et al. 2003). Given that induction of oxidative stress can have profound consequences on the cellular microenvironment and that the sustained oxidative insult has been shown to play a role in pathological processes, such as inflammation, cancer, and neurodegenerative diseases (Benhar et al. 2002; Roberts et al. 2009), understanding mechanisms through which high-dose BPA co-exposure might influence cell survival and cell death *in vitro* may improve our understanding of the potential consequences of low-dose environmental exposure to BPA.

In the present study, we examined the cellular microenvironment 4 h after BPA exposure, as in Gassman et al. 2015, and extended the analysis to 24 h after exposure. As in our previous study, a high-dose of BPA with a short exposure period was used to concentrate the effects of BPA and allow DNA damage and repair effects to be better monitored. Due to the efficiency and high catalytic responses of DNA repair proteins, a high dose/short duration exposure is often employed to better observe DNA repair proteins in action, and our BPA and $KBrO_3$ doses were selected with these parameters in mind. The high dose of BPA employed in this study was found to be minimally cytotoxicity with no observed increase in cell proliferation (Gassman et al. 2015). Increases in cell proliferation after exposure to BPA are frequently observed for low doses (Lapensee et al. 2009; Pfeifer et al. 2015); however, our 150 μM dose of BPA was not found to increase proliferation in the MEF model system used (Gassman et al. 2015), which is consistent with other high dose BPA studies (Ge et al. 2014; Samuelsen et al. 2001).

Whole-genome microarray analysis was performed to evaluate the global transcriptome changes associated with co-exposure of BPA and $KBrO_3$ at these two time points and to identify gene

targets induced by co-exposure that promote cell survival. Further, microenvironment changes in chromatin structure, glutathione content, and pH induced by exposure to BPA, $KBrO_3$, or both agents at these time points were also examined, to determine if an adaptive response is induced by co-exposure.

Material and Methods

Chemicals

BPA (Sigma Aldrich) was prepared in absolute ethanol and diluted to the final working concentration in medium. $KBrO_3$ was dissolved directly in the medium at the time of the experiment.

Cell culture

$Ku70^{-/-}$ mouse embryonic fibroblasts (MEFs) (a gift from Dr. Shigemi Matsuyama, Case Western University, Cleveland, OH) were grown at 37 °C in a 10 % CO_2 incubator in Dulbecco's modified Eagle's medium (DMEM) supplemented with glutamine, 10 % fetal bovine serum (FBS; HyClone), 1 % non-essential amino acids, and 1 % sodium pyruvate (Gama et al. 2009). Cells were routinely tested and found to be free of mycoplasma contamination.

Cytotoxicity studies

Cytotoxicity was determined by growth inhibition assays. We consider this cell survival assay to be more reliable in MEFs than alternate assays such as clonogenic colony counting or short-term cell killing assays. Results obtained with the cell survival assay have been confirmed using other assays. Cells were seeded at a density of 40,000 cells/well in six-well dishes. The following day, cells were exposed to a range of concentrations of BPA alone for 25 h or $KBrO_3$ alone for 1 h. In

other cases, cells were exposed to 150 μM BPA for 1 h, then a range of $KBrO_3$ concentrations for 1 h, and finally with 150 μM BPA for a further 23 h. For $KBrO_3$ alone and BPA plus $KBrO_3$ co-exposures, after the 1 h $KBrO_3$ treatment, the cells were washed with Hanks' balanced salt solution (HBSS) and fresh medium was added with or without BPA. After 25 h exposure to BPA, cells were washed in HBSS and fresh medium was added. Dishes were then incubated for 6–7 days at 37°C in a 10% CO_2 incubator until untreated control cells were approximately 80% confluent. Cells (triplicate wells for each drug concentration) were counted by a cell lysis procedure (Butler 1984), and results were expressed as the number of cells in drug-treated wells relative to cells in control wells (% control growth).

RNA isolation

$Ku70^{-/-}$ cells were seeded in 145 mm dishes at 1×10^6 cells/dish and cultured to 80 % confluency. Cells were then treated with BPA, $KBrO_3$ or co-exposed to BPA and $KBrO_3$. $KBrO_3$ only cells were treated for 1 h with 20 mM $KBrO_3$, washed with HBSS, then fresh medium was added to cells. Cells were allowed to repair for an additional 3 or 23 h following treatment. For BPA only treatment, cells were incubated for 5 or 25 h in medium containing 150 μM BPA. For co-exposure, cell were incubated with 150 μM BPA for 1 h, then 20 mM $KBrO_3$ and 150 μM BPA for 1 h, washed with HBSS, then fresh medium with 150 μM BPA was added, and cells were allowed to repair for an additional 3 or 23 h. Since all treatments were conducted in parallel, the post-damage induction times throughout the manuscript refer to the initiation of $KBrO_3$ treatment, though no $KBrO_3$ was added to the BPA alone. 4 and 24 h after $KBrO_3$ treatment, cells were washed twice in phosphate buffered saline (PBS, Hyclone), and total cellular RNA was isolated using the RNeasy Midi Kit (Qiagen) according to the manufacturer's instructions. Residual genomic DNA was removed by on-column digestion with RNase-free DNase I

(Qiagen). Denaturing formaldehyde/agarose gel electrophoresis validated quality and integrity of RNA samples, and the samples were quantified by a Nanodrop ND-1000 spectrophotometer (Thermo Scientific), and purity was analyzed by the 260:280 absorbance ratio. Three biological replicates were collected and isolated for the control and for all the treatment conditions.

Microarray study

Gene expression analysis was performed using Agilent Whole Mouse Genome 4 × 44 multiplex format oligo arrays (Agilent Technologies) following the Agilent one-color microarray-based gene expression analysis protocol. Starting with 500 ng of total RNA, Cy3 labeled cRNA was produced according to manufacturer's protocol. For each sample, 1.65 µg of Cy3 labeled cRNA was fragmented and hybridized for 17 hours in a rotating hybridization oven. Slides were washed and then scanned with an Agilent Scanner. Data were obtained using the Agilent Feature Extraction software (v9.5), using the 1-color defaults for all parameters. The Agilent Feature Extraction Software performed error modeling, adjusting for additive and multiplicative noise. The resulting data were processed using Omicsoft Array Studio (Version 7.0) software. Significant probes were determined by filtering data to include only probes with fold changes greater than 1.5 or less than -1.5 over control and p values < 0.01, determined by an error-weighted one-way analysis of variance (ANOVA) and Bonferroni multiple test correction using the Omicsoft software. This list of differentially expressed genes generated by the Omicsoft software was used as an input for the curated pathway database, Ingenuity Pathway Analysis (IPA; Ingenuity® Systems; www.ingenuity.com). IPA's Core analysis module used the differentially expressed gene list to enrich for canonical and functional pathways or regulatory connections and to remove duplicates and unmapped genes. Significance values were calculated

using a right-tailed Fisher's exact test to determine if a pathway was overrepresented by calculating whether genes in a specific pathway were enriched within the data set compared to all genes on the array in the same pathway at a $p < 0.05$ cutoff for significance based on IPA threshold recommendations. Only pathways with a p value exceeding threshold and having more than two representative genes in the data set were considered. Final filtered gene lists generated by IPA were input into Partek® Genomic Suite software to create heat maps of hierarchical clustered genes and into http://www.pangloss.com/seidel/Protocols/venn.cgi to create Venn diagrams. Microarray intensity files can be accessed through Gene Expression Omnibus (http://www.ncbi.nlm.nih.gov/geo/) with the accession number GSE71489.

Chromatin condensation

The level of chromatin condensation was measured using the Hoechst, YO-PRO1, and propidium iodide (PI) dye stains from the Chromatin Condensation & Membrane Permeability Dead Cell Apoptosis Kit (Life Technologies) similar to (Muders et al. 2009). The intensity of Hoechst staining of DNA in compact chromatin regions, e.g. heterochromatin, is much more intense then Hoechst intercalated into looser regions of chromatin, e.g. euchromatin; therefore, difference in Hoechst intensity can be used to determine the degree of compaction observed across a nuclei (Belloc et al. 1994; Hinde et al. 2014; Mora-Bermudez and Ellenberg 2007; Zink et al. 2003). Examination of Hoechst intensity across nuclei with confocal microscopy has been used to observed chromatin dynamics in living cells, and here we extend this type of intensity measure with flow cytometry with the addition of YO-PRO1 and PI to identify apoptotic or necrotic cells during analysis. $Ku70^{-/-}$ cells were seeded in 100 mm dishes at 1×10^6 cells/dish, then treated on the following day with BPA, $KBrO_3$ or co-exposed, as described above. 4 or 24 h

after the initiation of $KBrO_3$ treatment, cells were harvested using 0.25 % trypsin, washed in 5 ml of PBS, and stained in 1 ml of PBS with 1 μL each of Hoechst 33342 stock solution, YO-PRO-1 stock solution, and PI stock solution at room temp for 15 min. Staurosporine treated cells were analyzed as a control for condensed chromatin. Cells were incubated with 2 μM staurosporine for 4 h at 37 °C, then harvested and stained as described for BPA, $KBrO_3$ or co-exposed samples. Stained cells were analyzed with Becton Dickinson LSRII flow cytometer (BD). The variations in Hoechst staining intensity in the live cells are plotted. The mean fluorescent intensity was reported for the Hoechst channel, which was the only channel to show staining and measurable changes in mean fluorescent intensity for BPA, KBrO3, and co-exposure conditions. Staurosporine treatment showed staining in all three channels. Mean intensities ± standard error of mean (SEM) for at least three experiments are reported.

Reduced glutathione assay

Levels of cellular reduced glutathione (GSH) were analyzed using ThiolTracker Violet GSH detection reagent® (Life Technologies) according to the manufacturer's protocol. $Ku70^{-/-}$ cells were seeded in 100 mm dishes at 1×10^6 cells/dish, and treated, as described above. 4 or 24 h after the initiation of $KBrO_3$ treatment, cells were harvested using 0.25 % trypsin, washed in 4 ml of PBS, and then stained in PBS containing 10 μM ThiolTracker Violet for 30 min at 37 °C. Stained cells were analyzed by flow cytometry on the LSRII, and the mean fluorescent intensity was recorded for ThiolTracker Violet. Mean intensities ± SEM of three experiments are reported.

pH measurement

Intracellular pH was quantified by flow cytometry with the pHRodo® Red AM Intracellular pH Indicator (Life Technologies) using the manufacturer's protocol. pHRodo is weakly fluorescent

at neutral pH and increasingly fluorescent in acidic pH, with a detectable pH range reported from 4 to 9. Ku70$^{-/-}$ cells were seeded in 100 mm dishes at 1×10^6 cells/dish, and then treated, as described above, with BPA, $KBrO_3$, or co-exposed to both agents. Additionally, for every experiment a calibration curve was prepared using the Intracellular pH Calibration Buffer Kit (Life Technologies). 4 or 24 h after the initiation of $KBrO_3$ treatment, cells were harvested using 0.25 % trypsin, washed in 4 ml of PBS, and stained with pHRodo® Red at 37 °C for 30 min. Cells were then washed twice in PBS, and the calibration curve samples were resuspended in valinomycin and nigericin with the pH calibration buffers of pH 5.5, 6.5, and 7.5 for 5 min prior to analysis, per the manufacturer's protocol. The addition of valinomycin and nigericin assists in the equilibration of the intracellular space with the pH buffer. Samples were then analyzed by flow cytometry on the LSRII, and the mean fluorescent intensity was recorded for pHRodo Red. A standard curve was prepared using the calibration buffer intensities, and the pH for the control and treated samples were calculated. Mean pH values ± SEM calculated for four experiments are reported.

Measurement of oxidatively induced DNA lesions

Gas chromatography/tandem mass spectrometry (GC-MS/MS) with isotope-dilution was used to identify and quantify modified DNA bases in DNA as described previously (Gassman et al. 2015).

Statistical Analysis

Measured DNA lesions are expressed as mean ± standard deviation (SD), and all other values are expressed as mean ± standard error of mean (SEM). The data were analyzed by means of

ANOVA and Turkey post hoc analysis. $p < 0.05$ denoted by * or † were considered to correspond with statistical significance.

Results

Whole genome microarray and pathway analysis To examine cellular changes induced by BPA, $KBrO_3$, and the co-exposure conditions, we performed whole genome microarray analysis of cells treated with BPA, $KBrO_3$ or co-exposed to BPA and $KBrO_3$. $KBrO_3$ only cells were treated for 1 h with 20 mM $KBrO_3$, washed, and allowed to repair for an additional 3 or 23 h following treatment. For BPA only treatment, cells were incubated for 5 or 25 h in medium containing 150 μM BPA. For co-exposure, cell were incubated with 150 μM BPA for 1 h, then 20 mM $KBrO_3$ and 150 μM BPA for 1 h, washed with HBSS, then fresh medium with 150 μM BPA was added, and cells were allowed to repair for an additional 3 or 23 h. Treatments were performed in parallel, and repair times after exposures are expressed relative to the initiation of $KBrO_3$ treatment, even though no $KBrO_3$ is added in the BPA alone exposure.

Gene lists were generated from the average of three biological replicates for each condition and significant probes were identified by selecting those probes showing p value < 0.01, determined by error-weighted ANOVA with Bonferroni multiple test correction. Duplicate reads and non-coding genes were removed by IPA software. At 4 h post-damage induction, 4007 unique genes were altered after treatment with $KBrO_3$, BPA or co-exposure, while 3144 unique gene changes were observed 24 h after damage induction. Figure 2A shows a heat map of the observed gene expression changes 4 h after treatment, while Figure 3A shows the observed changes at 24 h. Figure 2B shows a Venn diagram analysis of the gene list 4 h post-damage induction and

illustrates the common and unique gene expression changes among the treatment groups. Figure 3B shows the Venn diagram of these changes at 24 h post-damage induction.

At 4 h, 2008 genes were significantly different from controls after treatment with $KBrO_3$ only and with BPA + $KBrO_3$, and 569 genes were significantly different from controls after all 3 treatments (Figure 2). IPA was used to identify the top 5 networks that were significantly regulated in response to each treatment (Appendix 1, with networks ranked based on score and number of focus molecules), and the top 5 up-regulated and top 5 down-regulated genes for each treatment are shown in Table 2 (with rankings based fold change over control with a $p < 0.01$). Appendix 2 and Table 3 show the top ranked networks and induced and repressed genes observed after 24 h. There are no common top networks associated with each treatment at 4 or 24 h; however, there are common top genes induced or repressed at each time period. $KBrO_3$ alone and co-exposed with BPA both show up-regulation of GSTA5 at both 4 and 24 h, while up-regulation of IL18R is observed at 4 h, and up-regulation of ROBO3 is observed at 24 h. Down-regulation of Cyp2d22 and Akr1b10 at 4 h and HP and CYP2F1 at 24 h is also observed for both $KBrO_3$ containing treatments. Up-regulation of EGR4 at 4 h is the only common gene observed for BPA alone and $KBrO_3$ alone treatments. Overall, each treatment condition altered network signaling and gene expression in a different manner, with the most overlap observed for the $KBrO_3$ and the co-exposure conditions, as illustrated by the heat maps and Venn diagrams (Figures 2 and 3).

There were 755 genes that were significantly different from controls in co-exposed cells at 4 h and 755 significant genes at 24 h, but only 86 genes were common to both time points. IPA was

performed on the 669 significant genes that were unique to co-exposed cells at 4h, and on the 669 significant genes that were unique to co-exposed cells at 24h, and the top 5 networks based on the unique genes at each time point are shown in Appendix 3.

Two of the top 5 networks identified by IPA that are unique to the co-exposure condition at 24 h are DNA Replication, Recombination networks (Appendix 3), and figure 4A and B show these networks. Genes regulated by co-exposure in these networks, include members of the base excision repair (BER), the nucleotide excision repair (NER), and double strand break repair pathways. To better understand the gene expression changes induced by the three treatment conditions after 24 h, we examined common DNA repair genes involved in the repair of oxidatively induced DNA damage from the BER, NER, and double strand break repair pathways (Table 4). After 24 h of BPA treatment alone, no significant gene expression changes over control were observed in these genes, with Rad51 being the only exception. $KBrO_3$ alone and co-exposure shows differential expression in these repair genes, with significant changes observed after co-exposure in the BER proteins Apex1, Lig3, Pnkp, Ogg1, and Tdp1 and in the NER proteins ERCC4, ERCC5, and ERCC8. Table 5 shows the gene expression levels of these genes 4 h after the induction of DNA damage with $KBrO_3$. As shown in Table 5, BPA alone again has little effect on the expression of DNA repair genes, while differential expression is observed for $KBrO_3$ alone and co-exposed with BPA. Interestingly, there is a suppression of a number genes involved in the removal of oxidatively induced DNA lesions, like Ogg1, Neil1, and Neil3, and genes involved in the subsequent gap filling reaction, Pol β and λ. With the exception of Ogg1, whose gene expression changes are observed at both 4 and 24 h, these changes are unique to the 4 h time point. These observed changes in gene expression at both 4 and 24 h are consistent with

BPA co-exposure inducing an adaptive response through gene regulation changes after the 4 h time point.

Chromatin condensation

Given the observed reduction in gene expression associated with BER and NER at 4 h, and our previous results indicating an increase in oxidatively induced DNA lesion coupled with a reduction in DNA strand breaks (Table 1) (Gassman et al. 2015), DNA repair may be altered during first 4 h of exposure, where repair of oxidatively induced DNA lesions typically occurs (Hollenbach et al. 1999; Jaruga and Dizdaroglu 1996). Chromatin structure has been demonstrated to regulate the access of DNA repair proteins to sites of DNA damage, and alterations in the chromatin structure has been shown to reduce excision of lesions, like 8-oxoGua (Amouroux et al. 2010).

To evaluate chromatin structure after BPA exposure and co-exposure, we used flow cytometry to examine the degree of compaction utilizing a DNA intercalating dye, Hoechst 33342. Hoechst 33342 brightly stains the condensed chromatin, e.g. heterochromatin, and dimly stains looser transcription ready chromatin, e.g. euchromatin, of live cells (Belloc et al. 1994; Khurana et al. 2014; Mora-Bermudez and Ellenberg 2007; Zink et al. 2003). In this assay, we measure the intensity of Hoechst staining in treated cells that are not undergoing apoptosis, as indicated by the lack of YO-PRO and PI staining, and any observed shift in the mean intensity of the Hoechst dye then reveals the degree of chromatin compaction induced by treatment (Figure 5). With this technique, compaction of chromatin was observed 4 h after treatment with BPA alone and co-exposure with BPA with $KBrO_3$ (156 % ± 12.5 % and 128 % ± 14.4 % of control, respectively).

This compaction may prevent DNA glycosylases from accessing oxidatively induced DNA lesions and is consistent with the lesion persistence and strand break signaling reduction previously reported (Gassman et al. 2015).

At 24 h, the degree of chromatin compaction for BPA treated cells was reduced significantly from the 4 h time point, but was still slightly higher than untreated cells (110 % ± 2.7 % of control). On the other hand, the $KBrO_3$ treated cells now show compaction (133 ± 5.3 % of control), indicating that $KBrO_3$ treated cells may be beginning to undergo apoptosis. Finally, co-exposed cells were consistent with untreated cells (99.6 ± 6.5 %).

Oxidative DNA damage

Previously, we determined that a significant amount of oxidatively induced DNA lesions persisted in the genomic DNA 4 h after DNA damage induction (Table 1 and (Gassman et al. 2015)), and this retention of lesions would be consistent with reduced access of DNA glycosylases to DNA lesions in condensed chromatin (Amouroux et al. 2010). Since this compaction was reduced 24 h after co-exposure, and the microarray analysis supports the up-regulation of DNA repair genes, we quantified oxidatively induced DNA lesions in DNA isolated from treated cells 24 h after damage induction, to determine if an increase in DNA lesions was still observed 24 h after treatment. GC-MS/MS with isotope-dilution, as described (Gassman et al. 2015; Reddy et al. 2013), was used to quantify lesions in isolated nuclear DNA. The mean values for the quantified DNA lesions are summarized in Table 6.

Our previous results showed a significant accumulation of lesions for BPA only (ThyGly) and for BPA and $KBrO_3$ co-exposure (ThyGly , FapyAde, and FapyGua) 4 h after damage induction (Table 1 and (Gassman et al. 2015)). Here, we observed no significant accumulation of lesions over control 24 h after damage induction. The ThyGly and FapyAde levels were consistent with or lower than control; the FapyGua levels reflect a slight, but non-significant, increase in lesion content over control; and 8-oxoGua shows a slight, but non-significant, decrease in lesion content. These results are consistent with the loss of oxidatively induce DNA lesions between 4 and 24 h.

Cellular GSH levels

In addition to generating oxidatively induced DNA lesions, exposure to oxidative stress can alter the cellular microenvironment and reduce the cellular redox balance. Depletion of intracellular glutathione has been previously observed after BPA exposure (Jain et al. 2011; Kabuto et al. 2003; Wu et al. 2013). To confirm that BPA alters the cellular microenvironment in a time-dependent manner, we measured depletion of intracellular GSH with a fluorescent dye, ThiolTracker Violet, which reacts with reduced thiols in live cells. At 4 h after exposure, the GSH levels in the treated cells were consistent with control, though a small shoulder in the mean intensity profile of the ThiolTracker dye appeared in both BPA samples; this indicates that GSH was beginning to be depleted because the fluorescent intensity of the ThiolTracker was being reduced in the cell population as a result (Figure 6). At 24 h after exposure, the GSH levels of cells exposed to BPA were reduced, and a clear second population was observed in the co-exposed cells (Figure 6, indicated by arrow). While the flow histograms show the appearance of a second population, a consistent gating could not be found for all treatments to reflect this

change in the mean intensity. Therefore, we have presented a representative histogram for the treatments, but also report that there are no significant changes observed in the average mean intensity over control for all treatments.

Intracellular pH

Induction of oxidative stress and depletion of intracellular GSH can also induce changes in intracellular pH. To determine the effect BPA exposure has on intracellular pH, we measured intracellular pH at 4 and 24 h after treatment (Table 7). At 4 h post-damage induction, $KBrO_3$ alone induced a significant shift in intracellular pH to 6.8. Treatment with BPA did not significantly alter the intracellular pH relative to untreated control. However, BPA co-exposure resulted in a pH of 7.0, which is significantly higher than the pH observed after $KBrO_3$ treatment ($p < 0.05$). At 24 h post-damage induction, the pH with $KBrO_3$ alone was similar to control, while the co-exposure condition is now significantly acidic compared to control and $KBrO_3$ alone treatment ($p < 0.05$). The delay in pH drop may be due to the depletion of GSH, as observed in Figure 6. Overall, the BPA co-exposure appears to mitigate the pH alterations induced by $KBrO_3$-induced oxidative stress at the 4 h time point.

Discussion

Numerous reports have indicated that BPA exposure induces global transcriptome and epigenetic changes that can have long-term consequences for cellular regulatory networks and signal transduction pathways (Bromer et al. 2010; Fernandez et al. 2012; Lee et al. 2008; Naciff et al. 2002; Patterson et al. 2015; Ptak et al. 2011; Tabuchi et al. 2006; Weng et al. 2010; Yin et al. 2014). While dosing conditions and exposure times can be highly variable in the literature, most

studies report alterations in DNA response and repair pathways, and a number of studies have demonstrated BPA exposure induces oxidative stress and oxidatively induced DNA lesions at both low environmentally relevant low doses (pM-nM) (Koong and Watson 2015; Pfeifer et al. 2015) and high dose of BPA (Babu et al. 2013; Gassman et al. 2015; Jain et al. 2011; Kabuto et al. 2003; Lee et al. 2008; Tiwari et al. 2012; Wu et al. 2013; Yang et al. 2009). Our previous work confirmed these results by demonstrating that high-dose BPA and $KBrO_3$ alone generated ROS and oxidatively induced DNA lesions (Table 1 and (Gassman et al. 2015)) and by demonstrating an increase in ROS after co-exposure, both through indirect measurement of the generated ROS and through measurement of the significant increase in oxidatively induced lesions (Gassman et al. 2015). However, features of how the cellular microenvironment reacts to the BPA-induced oxidative stress and responds to the induced DNA damage have been less well understood. Here, we present evidence that BPA exposure alters the microcellular environment to promote cell survival after the induction of additional oxidative stress by the oxidizing agent, $KBrO_3$.

Alteration of the chromatin structure through compaction and remodeling has been previously reported after oxidative stress induced by hydrogen peroxide (O'Hagan et al. 2011), $KBrO_3$ (Amouroux et al. 2010), and light activation of the KillerRed fluorescent protein (Lan et al. 2014). Further this compaction has been shown to reduce recruitment of the DNA glycosylase Ogg1, delaying the repair of oxidatively induced DNA lesions (Amouroux et al. 2010), and to promote the suppression of transcription and the accumulation of epigenetic marks silencing genes (O'Hagan et al. 2011). With high-dose BPA and $KBrO_3$ demonstrated to induce ROS species (Gassman et al. 2015), we evaluated the compaction of chromatin using Hoechst

staining. We observed a transient compaction of chromatin 4 h after exposure or co-exposure with BPA. This compaction may reduce the repair of oxidatively induced DNA lesions, reflected in an increased DNA lesion load consistent with our previous work (Gassman et al. 2015), and may promote the silencing of gene expression, consistent with the down-regulation of DNA repair proteins involved in BER observed in the microarray analysis (Table 5).

Coupled with the observed chromatin changes 4 h post-damage initiation, BPA co-exposure also significantly reduces the drop in intracellular pH observed after treatment with $KBrO_3$ alone (Table 7). Oxidative stress alters the balance intracellular redox machinery and can modify cellular membrane ion transport channels (Clerici et al. 1992). Changes in the cellular Na^+/H^+ antiporter activity and an increase in intracellular pH have been reported after exposure of estrogen and estradiol (Ediger et al. 1999; Incerpi et al. 2003; Kilic et al. 2009). Here, no increase in intracellular pH is observed after BPA exposure, and to our knowledge, no reports of intracellular pH changes with BPA exposure have been previously reported.

While depletion of GSH by ROS often results in changes in the cellular Na^+/H^+ antiporter activity and is associated with drop in intracellular pH (Ciriolo et al. 1997; Cutaia and Parks 1994), our conditions show no significant depletion of GSH at 4 h post-damage induction for any of our treatment conditions (Figure 6). The intracellular pH drop observed after $KBrO_3$ treatment is most likely the result of the increase in free K^+ released upon the formation of the reactive bromate anions. Effects of K^+ efflux from KCl exposure have been previously described in the literature (Adler and Fraley 1977), though our observation of a decrease in intracellular pH following $KBrO_3$ exposure is the first to our knowledge. There are numerous possible

explanations for how BPA exposure prevents the drop in intracellular pH, from activation of the mitogen-activated protein kinases (MAPK) pathway (Lee et al. 2008) to stimulation of the antiporter system. Further studies are needed to explore the mechanism by which BPA stabilizes against the drop in intracellular pH.

At 24 h post-damage induction, the suppressive aspects of BPA exposure observed at the 4 h time point have now transitioned into cellular microenvironment changes conducive to DNA repair. These changes would be consistent with an adaptive response being stimulated in the time period between 4 and 24 h that results in chromatin relaxation. Chromatin structure compaction, compared to control at 4 h, is now consistent with the control untreated cells; while $KBrO_3$ treated cells now show compact chromatin, which may reflect a progression toward apoptosis (Figure 5). The relaxation of chromatin is also reflected in the microarray results, where up-regulation of DNA repair genes involved in the repair of oxidatively induced DNA damage is observed (Table 4). Finally, the observed reduction in oxidatively induced DNA lesions at 24 h (Table 6) may reflect the promotion of DNA repair, though further work is required to establish the underlying mechanisms of repair utilized to remove the induced DNA lesions

Finally, 24 h post-damage initiation a slight, but not significant, reduction in GSH is observed in BPA exposed cells, and the intracellular pH of the co-exposed cells has dropped significantly compared to control; however, unlike the $KBrO_3$ only cells, the pH is still within values observed for control cells. GSH depletion has been previously observed after exposure to BPA and has been hypothesized to contribute to its pro-oxidant effects (Babu et al. 2013).

Together these results support a dynamic alteration of the cellular microenvironment that is initiated after co-exposure in our mouse fibroblast model system (Figure 7). While BPA exposure alone can alter gene expression (Bromer et al. 2010; Fernandez et al. 2012; Lee et al. 2008; Naciff et al. 2002; Patterson et al. 2015; Ptak et al. 2011; Tabuchi et al. 2006; Weng et al. 2010; Yin et al. 2014), deplete GSH (Jain et al. 2011; Kabuto et al. 2003; Wu et al. 2013), and induce oxidative stress in cells (Babu et al. 2013; Xin et al. 2014; Yang et al. 2009), this work demonstrates that high-dose BPA exposure coupled with endogenous or exogenous stresses, like $KBrO_3$-induced oxidative stress, can dramatically alter the microcellular environment and can delay and alter DNA damage response and repair.

These effects are largely uncharacterized in the literature, where focus has been on examining the endocrine disrupting functions of BPA or characterization of DNA damage effects of BPA exposure alone. To that point, it is important to note that our model system utilized normal serum. Our high dose/short duration model coupled with normal serum does not directly assay the interactions between BPA and estrogenic chemicals in the serum, nor does it exclude estrogen receptor mediated effects. However, since the observed cellular effects reported here are occurring in concert with these other exposure, it further emphasizes that mixture effects are complex and poorly understood. Despite the presence of competing estrogenic chemicals, our study still shows effects of BPA alone consist with a large body of previous reports (Babu et al. 2013; Jain et al. 2011; Kabuto et al. 2003; Nishimura et al. 2014; Wu et al. 2013; Xin et al. 2014; Yang et al. 2009), and our whole genome microarray, when compared with other published studies, shows consistency in the gene expression patterns for DNA repair proteins, inflammatory markers, and oxidative stress related genes that have observed at much lower doses

(Bromer et al. 2010; Fernandez et al. 2012; Lee et al. 2008; Naciff et al. 2002; Patterson et al. 2015; Ptak et al. 2011; Tabuchi et al. 2006; Weng et al. 2010; Yin et al. 2014).

Overall, the cellular responses to BPA co-exposure found here are striking, and it is clear from our results that BPA induces oxidative stress and promotes changes to the microcellular environment. These results, although in a selected cellular model optimized for the study DNA repair and damage response, have implications for the design of future animal and population-based studies.

We believe that our study highlights the importance of co-exposure effects, especially co-exposure with oxidative stress. The pro-oxidant activities of BPA and the adaptive response, identified here, indicate that BPA co-exposure may influence disease development and progression, particularly inflammatory diseases, which have been linked to BPA exposure (Bindhumol et al. 2003; Chitra et al. 2003; Yang et al. 2009). Future animal model and population-based studies should consider incorporating more oxidative stress and adaptive response indicators into their study design to better contextualize health effects of BPA.

Conclusions

In our Ku70-deficient mouse embryonic fibroblast model, co-exposure of high-dose BPA with the oxidizing agent $KBrO_3$ revealed evidence of changes to the cellular microenvironment that may indicate an adaptive response that promotes cell survival, despite an increase in oxidative stress. We interpret our observations as being consistent with underlying mechanisms whereby BPA exposed cells undergo an initial period of DNA repair suppression following exogenous

damage induction by $KBrO_3$, which is followed by an induced adaptive response, unique to the co-exposure condition, that results in whole genome expression changes, chromatin remodeling, depletion of intracellular GSH, and alterations in intracellular pH. However, although we believe that these hypothesized mechanisms are consistent with our observations, they need to be confirmed in other experimental models.

References

Adler S, Fraley DS. 1977. Potassium and intracellular pH. Kidney Int 11:433-442.

Amouroux R, Campalans A, Epe B, Radicella JP. 2010. Oxidative stress triggers the preferential assembly of base excision repair complexes on open chromatin regions. Nucleic Acids Res 38:2878-2890.

Babu S, Uppu S, Claville MO, Uppu RM. 2013. Prooxidant actions of bisphenol A (BPA) phenoxyl radicals: implications to BPA-related oxidative stress and toxicity. Toxicol Mech Methods 23:273-280.

Ballmaier D, Epe B. 2006. DNA damage by bromate: mechanism and consequences. Toxicology 221:166-171.

Belloc F, Dumain P, Boisseau MR, Jalloustre C, Reiffers J, Bernard P, et al. 1994. A flow cytometric method using Hoechst 33342 and propidium iodide for simultaneous cell cycle analysis and apoptosis determination in unfixed cells. Cytometry 17:59-65.

Benhar M, Engelberg D, Levitzki A. 2002. ROS, stress-activated kinases and stress signaling in cancer. EMBO Rep 3:420-425.

Bindhumol V, Chitra KC, Mathur PP. 2003. Bisphenol A induces reactive oxygen species generation in the liver of male rats. Toxicology 188:117-124.

Bromer JG, Zhou Y, Taylor MB, Doherty L, Taylor HS. 2010. Bisphenol-A exposure in utero leads to epigenetic alterations in the developmental programming of uterine estrogen response. FASEB J 24:2273-2280.

Butler WB. 1984. Preparing nuclei from cells in monolayer cultures suitable for counting and for following synchronized cells through the cell cycle. Anal Biochem 141:70-73.

Chitra KC, Latchoumycandane C, Mathur PP. 2003. Induction of oxidative stress by bisphenol A in the epididymal sperm of rats. Toxicology 185:119-127.

Choi YJ, Li H, Son MY, Wang XH, Fornsaglio JL, Sobol RW, et al. 2014. Deletion of Individual Ku Subunits in Mice Causes an NHEJ-Independent Phenotype Potentially by Altering Apurinic/Apyrimidinic Site Repair. PloS one 9:e86358.

Ciriolo MR, Palamara AT, Incerpi S, Lafavia E, Bue MC, De Vito P, et al. 1997. Loss of GSH, oxidative stress, and decrease of intracellular pH as sequential steps in viral infection. J Biol Chem 272:2700-2708.

Clerici C, Friedlander G, Amiel C. 1992. Impairment of sodium-coupled uptakes by hydrogen peroxide in alveolar type II cells: protective effect of d-alpha-tocopherol. Am J Physiol 262:L542-548.

Cutaia M, Parks N. 1994. Oxidant stress decreases Na+/H+ antiport activity in bovine pulmonary artery endothelial cells. Am J Physiol 267:L649-659.

Ediger TR, Kraus WL, Weinman EJ, Katzenellenbogen BS. 1999. Estrogen receptor regulation of the Na+/H+ exchange regulatory factor. Endocrinology 140:2976-2982.

Fernandez SV, Huang Y, Snider KE, Zhou Y, Pogash TJ, Russo J. 2012. Expression and DNA methylation changes in human breast epithelial cells after bisphenol A exposure. Int J Oncol 41:369-377.

Gama V, Gomez JA, Mayo LD, Jackson MW, Danielpour D, Song K, et al. 2009. Hdm2 is a ubiquitin ligase of Ku70-Akt promotes cell survival by inhibiting Hdm2-dependent Ku70 destabilization. Cell Death Differ 16:758-769.

Gassman NR, Coskun E, Stefanick DF, Horton JK, Jaruga P, Dizdaroglu M, et al. 2015. Bisphenol A promotes cell survival following oxidative DNA damage in mouse fibroblasts. PLoS One 10:e0118819.

Ge LC, Chen ZJ, Liu H, Zhang KS, Su Q, Ma XY, et al. 2014. Signaling related with biphasic effects of bisphenol A (BPA) on Sertoli cell proliferation: a comparative proteomic analysis. Biochim Biophys Acta 1840:2663-2673.

Hinde E, Kong X, Yokomori K, Gratton E. 2014. Chromatin dynamics during DNA repair revealed by pair correlation analysis of molecular flow in the nucleus. Biophys J 107:55-65.

Hollenbach S, Dhenaut A, Eckert I, Radicella JP, Epe B. 1999. Overexpression of Ogg1 in mammalian cells: effects on induced and spontaneous oxidative DNA damage and mutagenesis. Carcinogenesis 20:1863-1868.

Incerpi S, D'Arezzo S, Marino M, Musanti R, Pallottini V, Pascolini A, et al. 2003. Short-term activation by low 17beta-estradiol concentrations of the Na+/H+ exchanger in rat aortic smooth muscle cells: physiopathological implications. Endocrinology 144:4315-4324.

Iso T, Watanabe T, Iwamoto T, Shimamoto A, Furuichi Y. 2006. DNA damage caused by bisphenol A and estradiol through estrogenic activity. Biol Pharm Bull 29:206-210.

Jain S, Kumar CH, Suranagi UD, Mediratta PK. 2011. Protective effect of N-acetylcysteine on bisphenol A-induced cognitive dysfunction and oxidative stress in rats. Food Chem Toxicol 49:1404-1409.

Jaruga P, Dizdaroglu M. 1996. Repair of products of oxidative DNA base damage in human cells. Nucleic acids research 24:1389-1394.

Kabuto H, Hasuike S, Minagawa N, Shishibori T. 2003. Effects of bisphenol A on the metabolisms of active oxygen species in mouse tissues. Environ Res 93:31-35.

Khurana S, Kruhlak MJ, Kim J, Tran AD, Liu J, Nyswaner K, et al. 2014. A macrohistone variant links dynamic chromatin compaction to BRCA1-dependent genome maintenance. Cell Rep 8:1049-1062.

Kilic A, Javadov S, Karmazyn M. 2009. Estrogen exerts concentration-dependent pro-and anti-hypertrophic effects on adult cultured ventricular myocytes. Role of NHE-1 in estrogen-induced hypertrophy. J Mol Cell Cardiol 46:360-369.

Koong LY, Watson CS. 2015. Rapid, nongenomic signaling effects of several xenoestrogens involved in early- vs. late-stage prostate cancer cell proliferation. Endocrine Disruptors 3:e995003.

Lan L, Nakajima S, Wei L, Sun L, Hsieh CL, Sobol RW, et al. 2014. Novel method for site-specific induction of oxidative DNA damage reveals differences in recruitment of repair proteins to heterochromatin and euchromatin. Nucleic Acids Res 42:2330-2345.

Lapensee EW, Tuttle TR, Fox SR, Ben-Jonathan N. 2009. Bisphenol A at low nanomolar doses confers chemoresistance in estrogen receptor-alpha-positive and -negative breast cancer cells. Environ Health Perspect 117:175-180.

Lee S, Suk K, Kim IK, Jang IS, Park JW, Johnson VJ, et al. 2008. Signaling pathways of bisphenol A-induced apoptosis in hippocampal neuronal cells: role of calcium-induced reactive

oxygen species, mitogen-activated protein kinases, and nuclear factor-kappaB. J Neurosci Res 86:2932-2942.

Li H, Marple T, Hasty P. 2013. Ku80-deleted cells are defective at base excision repair. Mutat Res 745-746:16-25.

Mora-Bermudez F, Ellenberg J. 2007. Measuring structural dynamics of chromosomes in living cells by fluorescence microscopy. Methods 41:158-167.

Muders MH, Zhang H, Wang E, Tindall DJ, Datta K. 2009. Vascular endothelial growth factor-C protects prostate cancer cells from oxidative stress by the activation of mammalian target of rapamycin complex-2 and AKT-1. Cancer Res 69:6042-6048.

Naciff JM, Jump ML, Torontali SM, Carr GJ, Tiesman JP, Overmann GJ, et al. 2002. Gene expression profile induced by 17alpha-ethynyl estradiol, bisphenol A, and genistein in the developing female reproductive system of the rat. Toxicological sciences : an official journal of the Society of Toxicology 68:184-199.

Nishimura Y, Nakai Y, Tanaka A, Nagao T, Fukushima N. 2014. Long-term exposure of 3T3 fibroblast cells to endocrine disruptors alters sensitivity to oxidative injury. Cell biology international.

NTP. 2008. NTP-CERHR monograph on the potential human reproductive and developmental effects of bisphenol A. NTP CERHR MON:v, vii-ix, 1-64 passim.

O'Hagan HM, Wang W, Sen S, Destefano Shields C, Lee SS, Zhang YW, et al. 2011. Oxidative damage targets complexes containing DNA methyltransferases, SIRT1, and polycomb members to promoter CpG Islands. Cancer Cell 20:606-619.

Patterson AR, Mo X, Shapiro A, Wernke KE, Archer TK, Burd CJ. 2015. Sustained reprogramming of the estrogen response after chronic exposure to endocrine disruptors. Mol Endocrinol 29:384-395.

Pfeifer D, Chung YM, Hu MC. 2015. Effects of Low-Dose Bisphenol A on DNA Damage and Proliferation of Breast Cells: The Role of c-Myc. Environ Health Perspect.

Ptak A, Wróbel A, Gregoraszczuk EL. 2011. Effect of bisphenol-A on the expression of selected genes involved in cell cycle and apoptosis in the OVCAR-3 cell line. Toxicol Lett 202:30-35.

Reddy PT, Jaruga P, Kirkali G, Tuna G, Nelson BC, Dizdaroglu M. 2013. Identification and quantification of human DNA repair protein NEIL1 by liquid chromatography/isotope-dilution tandem mass spectrometry. J Proteome Res 12:1049-1061.

Roberts RA, Laskin DL, Smith CV, Robertson FM, Allen EM, Doorn JA, et al. 2009. Nitrative and oxidative stress in toxicology and disease. Toxicol Sci 112:4-16.

Roth RB, Samson LD. 2002. 3-Methyladenine DNA glycosylase-deficient Aag null mice display unexpected bone marrow alkylation resistance. Cancer Res 62:656-660.

Samuelsen M, Olsen C, Holme JA, Meussen-Elholm E, Bergmann A, Hongslo JK. 2001. Estrogen-like properties of brominated analogs of bisphenol A in the MCF-7 human breast cancer cell line. Cell Biol Toxicol 17:139-151.

Sobol RW, Kartalou M, Almeida KH, Joyce DF, Engelward BP, Horton JK, et al. 2003. Base excision repair intermediates induce p53-independent cytotoxic and genotoxic responses. J Biol Chem 278:39951-39959.

Tabuchi Y, Takasaki I, Kondo T. 2006. Identification of genetic networks involved in the cell injury accompanying endoplasmic reticulum stress induced by bisphenol A in testicular Sertoli cells. Biochem Biophys Res Commun 345:1044-1050.

Tiwari D, Kamble J, Chilgunde S, Patil P, Maru G, Kawle D, et al. 2012. Clastogenic and mutagenic effects of bisphenol A: an endocrine disruptor. Mutat Res 743:83-90.

Vandenberg LN, Hauser R, Marcus M, Olea N, Welshons WV. 2007. Human exposure to bisphenol A (BPA). Reprod Toxicol 24:139-177.

Vandenberg LN, Chahoud I, Heindel JJ, Padmanabhan V, Paumgartten FJ, Schoenfelder G. 2010. Urinary, circulating, and tissue biomonitoring studies indicate widespread exposure to bisphenol A. Environ Health Perspect 118:1055-1070.

Vandenberg LN. 2014. Non-monotonic dose responses in studies of endocrine disrupting chemicals: bisphenol a as a case study. Dose Response 12:259-276.

Weng YI, Hsu PY, Liyanarachchi S, Liu J, Deatherage DE, Huang YW, et al. 2010. Epigenetic influences of low-dose bisphenol A in primary human breast epithelial cells. Toxicol Appl Pharmacol 248:111-121.

Wu HJ, Liu C, Duan WX, Xu SC, He MD, Chen CH, et al. 2013. Melatonin ameliorates bisphenol A-induced DNA damage in the germ cells of adult male rats. Mutat Res 752:57-67.

Xin F, Jiang L, Liu X, Geng C, Wang W, Zhong L, et al. 2014. Bisphenol A induces oxidative stress-associated DNA damage in INS-1 cells. Mutat Res Genet Toxicol Environ Mutagen 769:29-33.

Yang YJ, Hong YC, Oh SY, Park MS, Kim H, Leem JH, et al. 2009. Bisphenol A exposure is associated with oxidative stress and inflammation in postmenopausal women. Environ Res 109:797-801.

Yin R, Gu L, Li M, Jiang C, Cao T, Zhang X. 2014. Gene expression profiling analysis of bisphenol A-induced perturbation in biological processes in ER-negative HEK293 cells. PLoS One 9:e98635.

Zink D, Sadoni N, Stelzer E. 2003. Visualizing chromatin and chromosomes in living cells. Methods 29:42-50.

Table 1. Measured oxidatively damaged DNA bases in Ku70$^{-/-}$ genomic DNA 4 h post-damage induction[a] (adapted from Gassman et al. 2015).

Exposure	DNA lesion/ 10^6 DNA bases (mean ± SD, n >3)[b]			
	ThyGly	FapyAde	FapyGua	8-oxoGua
Control	3.82 ± 1.32	2.83 ± 0.98	3.69 ± 1.41	0.98 ± 0.16
BPA	8.41 ± 0.45*	3.72 ± 1.37	5.19 ± 0.92	1.21 ± 0.4
$KBrO_3$	5.11 ± 0.69	4.01 ± 0.86	4.6 ± 0.92	1.33 ± 0.55
BPA + $KBrO_3$	7.48 ± 0.48*†	4.38 ± 0.41*	6.77 ± 1.36*†	1.55 ± 0.59

[a]150 μM BPA only was exposed for 5 h, 20 mM of $KBrO_3$ only was exposed for 4 h, and for co-exposure 150 μM BPA was exposed for 1 h, then 150 μM BPA + 20 mM of $KBrO_3$ only was exposed for 1 h, followed by 3 h of 150 μM BPA only

[b]measurements were made by GC/MS as described in Materials and Methods

*$p < 0.05$ compared with untreated controls, † $p < 0.05$ compared with $KBrO_3$

Table 2. Top 5 up-regulated and top 5 down-regulated genes ranked by magnitude of fold change over control at 4 h post-damage induction[a]

Outcome	BPA		$KBrO_3$		BPA + $KBrO_3$	
	Gene	Fold Change[b]	Gene	Fold Change	Gene	Fold Change
Up-regulated						
	CCL20	60.37	GSTA5	195.423	IL18R1	150.272
	CXCL3	55.581	IL18R1	165.986	GSTA5	118.712
	Saa3	26.361	AREG	131.227	PTGS2	95.172
	HCAR2	25.405	DUSP2	92.477	AREG	84.638
	EGR4	23.721	EGR4	65.351	ATF3	81.49
Down-regulated						
	LGALS12	-10.284	KLF15	-56.007	TNS1	-41.975
	DSC1	-8.749	Cyp2d22	-35.115	Akr1b10	-39.628
	FRY	-5.689	IKZF2	-22.961	FZD2	-35.905
	HPGD	-4.937	BMF	-22.292	Cyp2d22	-35.268
	PLCH2	-4.768	Akr1b10	-21.197	KAT2B	-30.719

[a]150 μM BPA only was exposed for 5 h, 20 mM of $KBrO_3$ only was exposed for 4 h, and for co-exposure 150 μM BPA was exposed for 1 h, then 150 μM BPA + 20 mM of $KBrO_3$ only was exposed for 1 h, followed by 3 h of 150 μM BPA only

[b]Gene expression fold change was evaluated compared to untreated control with all p values <0.01

Table 3. Top 5 up-regulated and top 5 down-regulated genes ranked by magnitude of fold change over control at 24 h post-damage induction[a]

Outcome	BPA		$KBrO_3$		BPA + $KBrO_3$	
	Gene	Fold Change[b]	Gene	Fold Change	Gene	Fold Change
Up-regulated						
	Wfdc17	37.229	GSTA5	87.219	GSTA5	181.836
	Saa3	25.573	ROBO3	22.114	Prg4	62.482
	LCN2	19.522	Prg4	16.538	ROBO3	59.949
	OSTN	16.42	BLNK	15.8	MMP15	25.597
	CA6	15.788	PTPN22	15.395	CA6	23.355
Down-regulated						
	MYH1	-11.145	FGL2	-73.599	AGTR2	-153.275
	Nebl	-10.875	CYP2F1	-59.905	HP	-125.757
	MYH2	-9.608	SLCO2B1	-57.705	DIO3	-114.982
	SLC26A7	-9.425	VIT	-55.675	SLCO2B1	-102.011
	NPR3	-9.109	HP	-37.549	CYP2F1	-85.326

[a]150 μM BPA only was exposed for 25 h, 20 mM of $KBrO_3$ only was exposed for 24 h, and for co-exposure 150 μM BPA was exposed for 1 h, then 150 μM BPA + 20 mM of $KBrO_3$ only was exposed for 1 h, followed by 23 h of 150 μM BPA only

[b]Gene expression fold change was evaluated compared to untreated control with all p values <0.01

Table 4. Selected DNA repair genes identified at 24 h post-damage induction[a], with the magnitude of the fold change over control for genes with p values < 0.05.

BPA	Fold Change[b]	$KBrO_3$	Fold Change	BPA + $KBrO_3$	Fold Change
Apex1	n.c.	Apex1	1.67	Apex1	1.82
Ercc3	n.c.	Ercc3	2.09	Ercc3	1.86
Ercc5	n.c.	Ercc5	n.c.	Ercc5	1.85
Ercc6	n.c.	Ercc6	1.91	Ercc6	n.c.
Ercc8	n.c.	Ercc8	2.30	Ercc8	2.5
Exo1	n.c.	Exo1	2.14	Exo1	2.19
Fen1	n.c.	Fen1	2.64	Fen1	2.40
Lig3	n.c.	Lig3	n.c.	Lig3	2.02
Lig4	n.c.	Lig4	1.88	Lig4	n.c.
Mre11	n.c.	Mre11	2.89	Mre11	2.27
Mutyh	n.c.	Mutyh	2.22	Mutyh	1.64
Ogg1	n.c.	Ogg1	n.c.	Ogg1	1.86
Parp1	n.c.	Parp1	1.93	Parp1	1.68
Rad51	1.83	Rad51	2.13	Rad51	2.35
Rpa1	n.c.	Rpa1	1.47	Rpa1	2.35
Tdg1	n.c.	Tdg1	2.15	Tdg1	2.10
Tdp1	n.c.	Tdp1	1.44	Tdp1	1.66
Genes unique to 24 h					
Atm	n.c.	Atm	1.64	Atm	1.89
Brca1	n.c.	Brca1	2.62	Brca1	2.0
Ercc1	n.c.	Ercc1	2.07	Ercc1	1.70
Ercc4	n.c.	Ercc4	3.15	Ercc4	4.05
Pnkp	n.c.	Pnkp	n.c.	Pnkp	2.05
Pol δ	n.c.	Pol δ	n.c.	Pol δ	1.68
Pol κ	n.c.	Pol κ	n.c.	Pol κ	1.68
Rad50	n.c.	Rad50	1.58	Rad50	1.69
Xrcc5	n.c.	Xrcc5	n.c.	Xrcc5	1.92

n.c. – no significant change over control

[a]150 μM BPA only was exposed for 25 h, 20 mM of $KBrO_3$ only was exposed for 24 h, and for co-exposure 150 μM BPA was exposed for 1 h, then 150 μM BPA + 20 mM of $KBrO_3$ only was exposed for 1 h, followed by 23 h of 150 μM BPA only

[b]Gene expression fold change was evaluated compared to untreated control with all p values <0.05

Table 5. Selected DNA repair genes identified 4 h post-damage induction[a], with the magnitude of the fold change over control for genes with p values < 0.05.

BPA	Fold Change[b]	$KBrO_3$	Fold Change	BPA + $KBrO_3$	Fold Change
Apex1	n.c.	Apex1	n.c.	Apex1	1.58
Ercc3	n.c.	Ercc3	n.c.	Ercc3	1.45
Ercc5	n.c.	Ercc5	-1.49	Ercc5	n.c.
Ercc6	n.c.	Ercc6	n.c.	Ercc6	2.62
Ercc8	n.c.	Ercc8	4.63	Ercc8	6.36
Exo1	1.6	Exo1	2.33	Exo1	3.4
Fen1	n.c.	Fen1	1.73	Fen1	1.9
Lig3	n.c.	Lig3	n.c.	Lig3	2.02
Lig4	n.c.	Lig4	n.c.	Lig4	2.4
Mre11	n.c.	Mre11	n.c.	Mre11	2.27
Mutyh	n.c.	Mutyh	-3.33	Mutyh	-2.2
Ogg1	n.c.	Ogg1	-1.68	Ogg1	-2.0
Parp1	n.c.	Parp1	-1.28	Parp1	-1.39
Rad51	1.83	Rad51	-3.11	Rad51	-2.49
Rpa1	n.c.	Rpa1	1.56	Rpa1	1.53
Tdg1	n.c.	Tdg1	2.12	Tdg1	2.82
Tdp1	n.c.	Tdp1	1.44	Tdp1	1.66
Genes unique to 4 h					
Mpg	n.c.	Mpg	-1.91	Mpg	-2.59
Neil1	n.c.	Neil1	-2.48	Neil1	-2.46
Neil3	n.c.	Neil3	-6.24	Neil3	-11.36
Pol β	n.c.	Pol β	n.c.	Pol β	-2.90
Pol λ	n.c.	Pol λ	-3.49	Pol λ	-2.92
Xrcc1	n.c.	Xrcc1	-1.72	Xrcc1	-1.76

n.c. – no significant change over control

[a]150 μM BPA only was exposed for 25 h, 20 mM of $KBrO_3$ only was exposed for 24 h, and for co-exposure 150 μM BPA was exposed for 1 h, then 150 μM BPA + 20 mM of $KBrO_3$ only was exposed for 1 h, followed by 23 h of 150 μM BPA only

[b]Gene expression fold change was evaluated compared to untreated control with all p values <0.05

Table 6. Levels of oxidatively induced DNA bases in Ku70$^{-/-}$ genomic DNA 24 h after damage induction[a]

Exposure	DNA lesion/ 10^6 DNA bases (mean ± SD, n >3)[b]			
	ThyGly	FapyAde	FapyGua	8-oxoGua
Control	5.32 ± 0.80	3.61 ± 0.26	3.81 ± 0.83	3.25 ± 0.01
BPA	2.54 ± 0.69	2.75 ± 1.74	3.71 ± 1.88	3.09 ± 0.57
$KBrO_3$	3.54 ± 0.27	3.21± 0.32	3.77 ± 1.31	2.84 ± 0.55
BPA + $KBrO_3$	5.38 ± 1.74	3.35 ± 0.31	6.00 ± 2.02	2.80 ± 0.80

[a]150 μM BPA only was exposed for 25 h, 20 mM of $KBrO_3$ only was exposed for 24 h, and for co-exposure 150 μM BPA was exposed for 1 h, then 150 μM BPA + 20 mM of $KBrO_3$ only was exposed for 1 h, followed by 23 h of 150 μM BPA only

[b]measurements were made by GC/MS as described in Materials and Methods

Table 7. Intracellular pH[a] in controls and in treated cells (mean ± SD)

Exposure	4 h[b]	24 h[b]
Control	7.5 ± 0.11	7.5 ± 0.08
BPA	7.5 ± 0.28	7.5 ± 0.11
$KBrO_3$	6.8 ± 0.11 *	7.8 ± 0.26
BPA + $KBrO_3$	7.2 ± 0.08†	7.0 ± 0.14 *†

[a]Intracellular pH was quantified by flow cytometry using the pHRodo

[b]150 µM BPA only was exposed for 5 or 25 h, 20 mM of $KBrO_3$ only was exposed for 4 or 24 h, and for co-exposure 150 µM BPA was exposed for 1 h, then 150 µM BPA + 20 mM of $KBrO_3$ only was exposed for 1 h, followed by 3 or 23 h of 150 µM BPA only

*$p < 0.05$ compared with untreated controls, † $p < 0.05$ compared with KBrO3 alone

Appendix 1. Top regulated networks[a] 4 h post-damage induction[b]

$KBrO_3$

1. Cell Morphology, Cellular Assembly and Organization, Cellular Function and Maintenance

2. Cancer, Organismal Injury and Abnormalities, Reproductive System Disease

3. Hereditary Disorder, Neurological Disease, Lipid Metabolism

4. Cell-To-Cell Signaling and Interaction, Cellular Function and Maintenance, Hematological System Development and Function

5. Protein Synthesis, RNA Post-Transcriptional Modification, Carbohydrate Metabolism

BPA

1. Cellular Development, Cellular Growth and Proliferation, Organ Development

2. Cellular Movement, Immune Cell Trafficking, Connective Tissue Disorders

3. Cellular Development, Cellular Growth and Proliferation, Connective Tissue Development and Function

4. Neurological Disease, Cell-To-Cell Signaling and Interaction, Hematological System Development and Function

5. Dermatological Diseases and Conditions, Organismal Injury and Abnormalities, Lipid Metabolism

BPA + $KBrO_3$

1. Embryonic Development, Nervous System Development and Function, Organ Development

2. Cellular Growth and Proliferation, Infectious Disease, Protein Synthesis

3. Cell Cycle, Cellular Assembly and Organization, Reproductive System Development and Function

4. Developmental Disorder, Hereditary Disorder, Metabolic Disease

5. Organismal Development, Tissue Morphology, Drug Metabolism

[a]Ranked by IPA by score and number of focus molecules

[b]150 μM BPA only was exposed for 5 h, 20 mM of $KBrO_3$ only was exposed for 4 h, and for co-exposure 150 μM BPA was exposed for 1 h, then 150 μM BPA + 20 mM of $KBrO_3$ only was exposed for 1 h, followed by 3 h of 150 μM BPA only

Appendix 2. Top regulated networks[a] 24 h after damage induction[b]

$KBrO_3$

1. Cardiovascular System Development and Function, Cellular Movement, Cancer
2. Cell Death and Survival, Dermatological Diseases and Conditions, Developmental Disorder
3. Gastrointestinal Disease, Hepatic System Disease, Liver Cirrhosis
4. Cell Death and Survival, Drug Metabolism, Endocrine System Development and Function
5. Cancer, Organismal Injury and Abnormalities, Connective Tissue Disorders

BPA

1. Cellular Movement, Connective Tissue Development and Function, Organ Morphology
2. Connective Tissue Disorders, Organismal Injury and Abnormalities, Skeletal and Muscular Disorders
3. Cardiac Dysfunction, Cardiovascular Disease, Organismal Injury and Abnormalities
4. Organismal Development, Energy Production, Molecular Transport
5. Cell-To-Cell Signaling and Interaction, Cellular Movement, Hematological System Development and Function

BPA + $KBrO_3$

1. Dermatological Diseases and Conditions, Inflammatory Disease, Skeletal and Muscular Disorders
2. Amino Acid Metabolism, Small Molecule Biochemistry, Neurological Disease
3. Protein Synthesis, Cell Death and Survival, Embryonic Development
4. Cancer, Embryonic Development, Cellular Development
5. Cell Cycle, DNA Replication, Recombination, and Repair, Cancer

[a]Ranked by IPA by score and number of focus molecules

[b]150 µM BPA only was exposed for 25 h, 20 mM of $KBrO_3$ only was exposed for 24 h, and for co-exposure 150 µM BPA was exposed for 1 h, then 150 µM BPA + 20 mM of $KBrO_3$ only was exposed for 1 h, followed by 23 h of 150 µM BPA only

Appendix 3. Top networks[a] regulated by the unique co-exposure genes at 4 and 24 h after damage induction[b,c]

4h

1. Nervous System Development and Function, Organ Morphology, Organismal Development
2. Energy Production, Nucleic Acid Metabolism, Small Molecule Biochemistry
3. Developmental Disorder, Hereditary Disorder, Metabolic Disease
4. RNA Post-Transcriptional Modification, Cancer, Hematological Disease
5. Connective Tissue Disorders, Skeletal and Muscular Disorders, Developmental Disorder

24 h

1. DNA Replication, Recombination, and Repair, Hereditary Disorder, Neurological Disease
2. Cancer, Gastrointestinal Disease, Hepatic System Disease
3. DNA Replication, Recombination, and Repair, Cellular Response to Therapeutics, Cell Cycle
4. Gene Expression, Cancer, Hereditary Disorder
5. Nucleic Acid Metabolism, Small Molecule Biochemistry, Amino Acid Metabolism

[a]Ranked by IPA by score and number of focus molecules

[b]150 μM BPA only was exposed for 5 h, 20 mM of $KBrO_3$ only was exposed for 4 h, and for co-exposure 150 μM BPA was exposed for 1 h, then 150 μM BPA + 20 mM of $KBrO_3$ only was exposed for 1 h, followed by 3 h of 150 μM BPA only

[c]150 μM BPA only was exposed for 25 h, 20 mM of $KBrO_3$ only was exposed for 24 h, and for co-exposure 150 μM BPA was exposed for 1 h, then 150 μM BPA + 20 mM of $KBrO_3$ only was exposed for 1 h, followed by 23 h of 150 μM BPA only

Figure Legends

Figure 1. Cell survival following co-exposure of BPA and $KBrO_3$ (adapted from Gassman et al. 2015). Ku70-deficient cells were treated with increasing amounts of $KBrO_3$ for 1 h (solid circles) or pre-treated with 150 μM BPA for 1 h, co-exposed with BPA and increasing amounts of $KBrO_3$ for 1 h, then BPA exposure was continued for a total of 24 h after $KBrO_3$ exposure (open circles). After 24 h, cells were washed and fresh medium was applied and they were allowed to grow for 6-7 days. Cells were counted and inhibition of growth was determined as the number cells remaining after treatment compared to control (% Control).

Figure 2. Gene expression changes observed by whole genome analysis of mRNA isolated 4 h after treatment with $KBrO_3$, BPA, or co-exposure of both agents, as described in Material and Methods. (A) Heat map of gene expression changes observed after treatment was generated using Partek® Genomic Suite software with probes selected by a fold change cutoff of ± 1.5 compared to untreated controls and an ANOVA-calculated significance level of $p < 0.01$ (n = 3). (B) Significant probe changes identified using the described criteria are sorted by Venn diagram.

Figure 3. Gene expression changes observed by whole genome analysis of mRNA isolated 24 h after treatment with $KBrO_3$, BPA, or co-exposure of both agents, as described in Material and Methods. (A) Heat map of gene expression changes observed after treatment was generated using Partek® Genomic Suite software with probes selected by a fold change cutoff of ± 1.5 compared to untreated controls and an ANOVA-calculated significance level of $p < 0.01$ (n = 3). (B) Significant probe changes identified using the described criteria are sorted by Venn diagram.

Figure 4. DNA replication, recombination, and repair networks identified from the uniquely regulated genes identified for the co-exposure condition 24 h after damage induction by IPA's core analysis module, which searches for enriched canonical pathways. (A) DNA replication, recombination, and repair network 1 (score 46, 31 focus molecules, p value of top functions 7.18E-05) is presented with expression values for the co-exposure overlaid, as an indicator of up- or down-regulation (red and green, respectively). (B) DNA replication, recombination, and repair network 3 (score 38, 28 focus molecules, p value of top functions 4.458E-08) is presented with expression values for the co-exposure overlaid, as an indicator of up- or down-regulation (red and green, respectively).

Figure 5. Levels of chromatin condensation after treatment with $KBrO_3$, BPA, or co-exposure of both agents at 4 and 24 h post-damage induction were measured by intensity of Hoechst and PI staining using flow cytometry. (A) Hoechst and PI stained live cells are sorted by intensity, and the contour maps of the measured intensities for a representative experiment at 4 and 24 h are shown. Dashed line shows the center of the control contour plot and highlights changes relative to the control cells. (B) Mean intensities values of the Hoechst staining for each treatment condition 4 h post-damage induction normalized to the control are shown (mean ± SEM of 3 biological replicates). (C) Mean intensities of the Hoechst staining for each treatment condition 24 h post-damage induction normalized to the control are shown (mean ± SEM). $*p < 0.05$, with solid and dashed lines showing comparison groups.

Figure 6. Levels of free GSH after treatment with $KBrO_3$, BPA, or co-exposure of both agents at 4 and 24 h post-damage induction were measured by staining live cells with ThiolTracker Violet and sorting by flow cytometry. (A) ThiolTracker Violet live cells are sorted by intensity and the measured intensities for a representative experiment at 4 and 24 h are shown. Dashed line indicated the center of the intensity peak for the control cells and highlights the relative changes in measured intensity compared to the control cells. The long white arrows indicate the direction of decreasing GSH measured by loss of dye intensity. The short white arrow indicates the subpopulation reflecting lower GSH content. (B) Mean intensities values of the ThiolTracker Violet staining for each treatment condition 4 h (black) and 24 h (red) after damage induction normalized to the control are shown (mean ± SEM of 3 replicates).

Figure 7. Proposed time-line for the cellular changes observed after BPA exposure based on our findings. We hypothesize that DNA repair is inhibited, both the recognition and excision level, and at the transcription level, up to 4 h after treatment with BPA (in BPA only cells) or with $KBrO_3$ (in co-exposed cells), and that between 4 and 24 h, an adaptive response is induced by BPA co-exposure that results in the up-regulation of DNA repair networks, while alterations in the cellular microenvironment are induced through pH changes and anti-oxidant depletion. Such changes might result in long-term epigenetic changes or reprogramming events.

Figure 1.

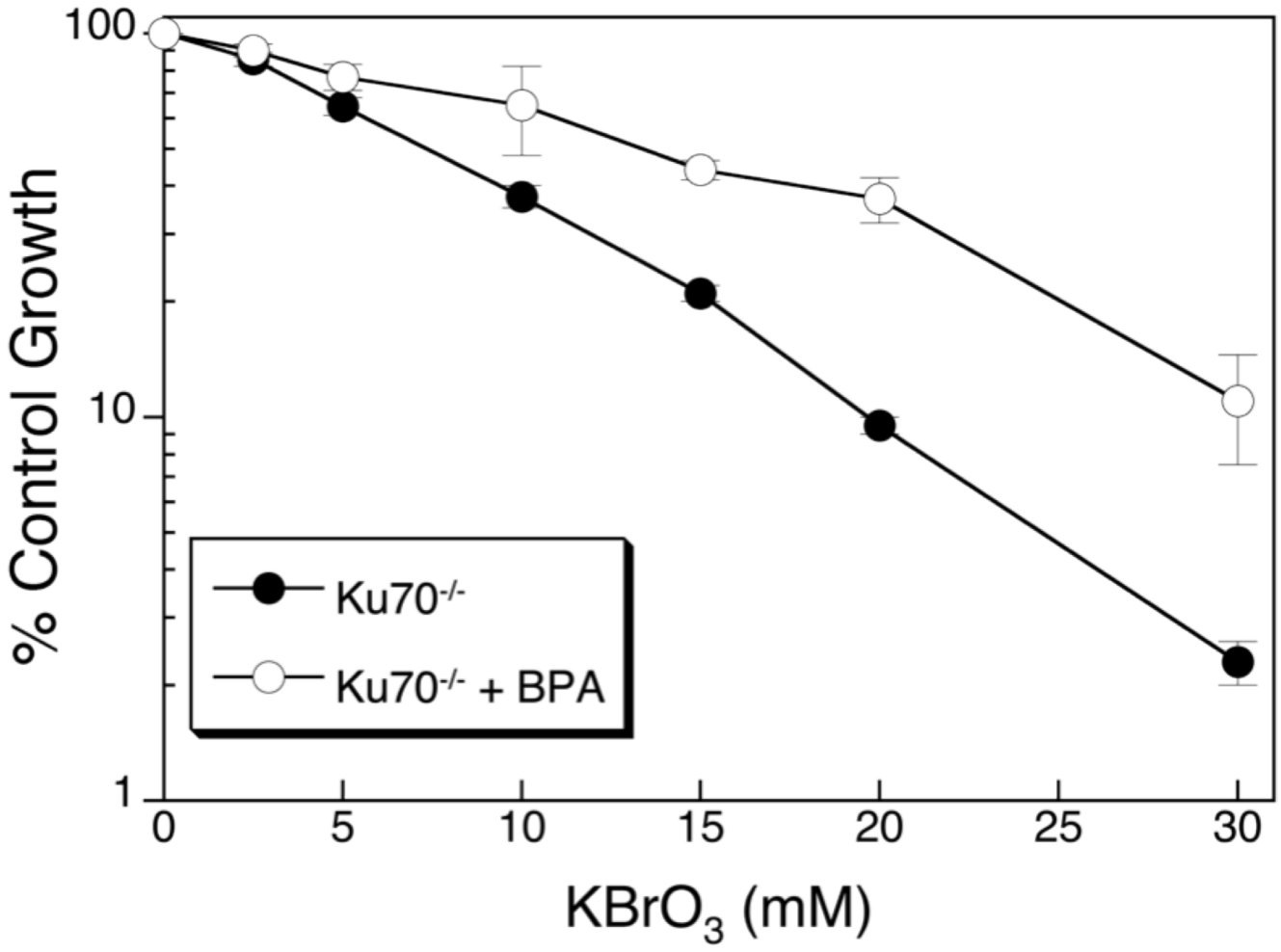

Figure 2.

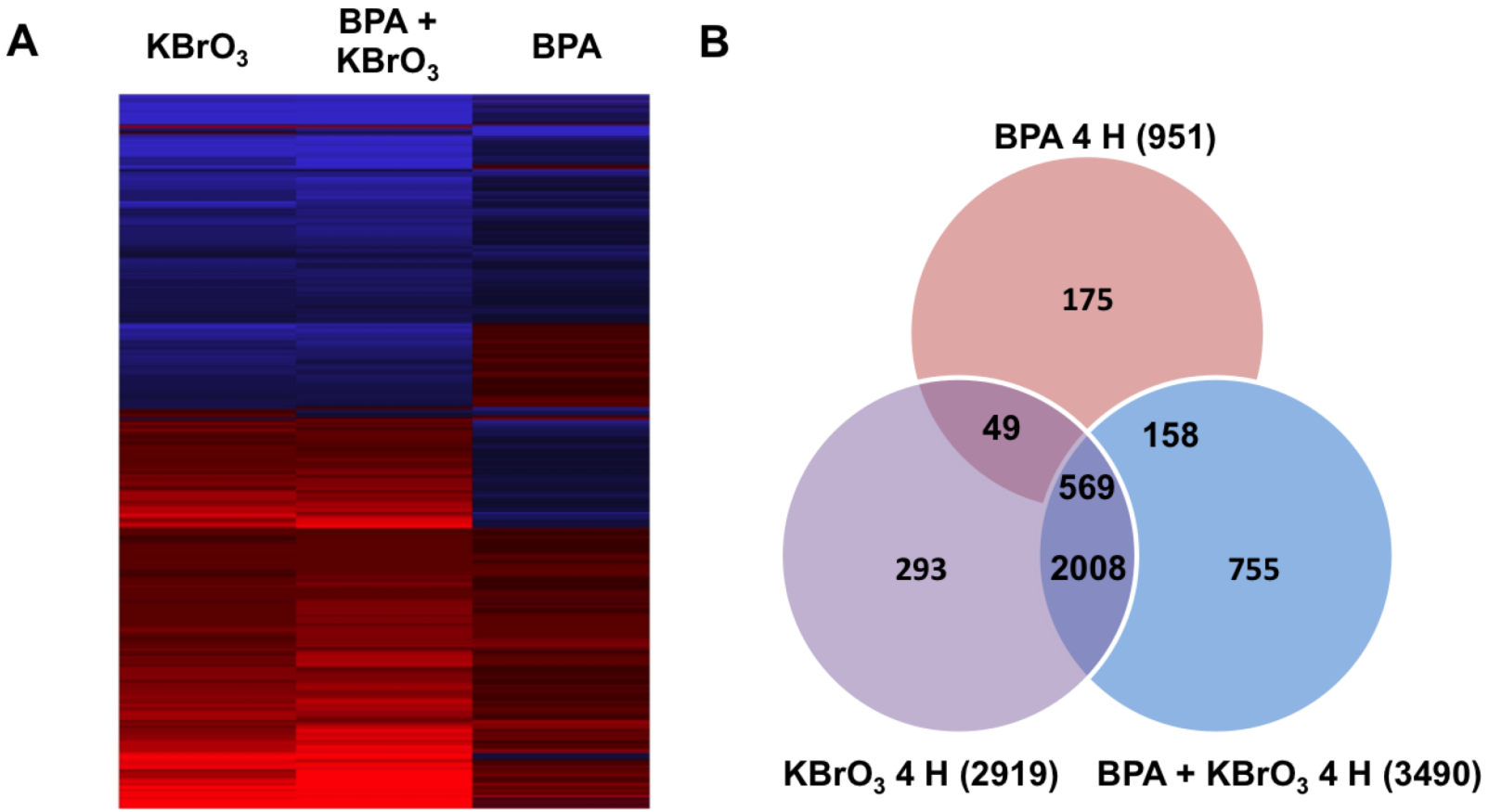
A
KBrO3
BPA + KBrO3
BPA
Minimum
Maximum
Fold Change
-5.00
0.00
5.00
B
BPA 4 H (951)
175
49
158
569
293
2008
755
KBrO3 4 H (2919)
BPA + KBrO3 4 H (3490)

Figure 3.

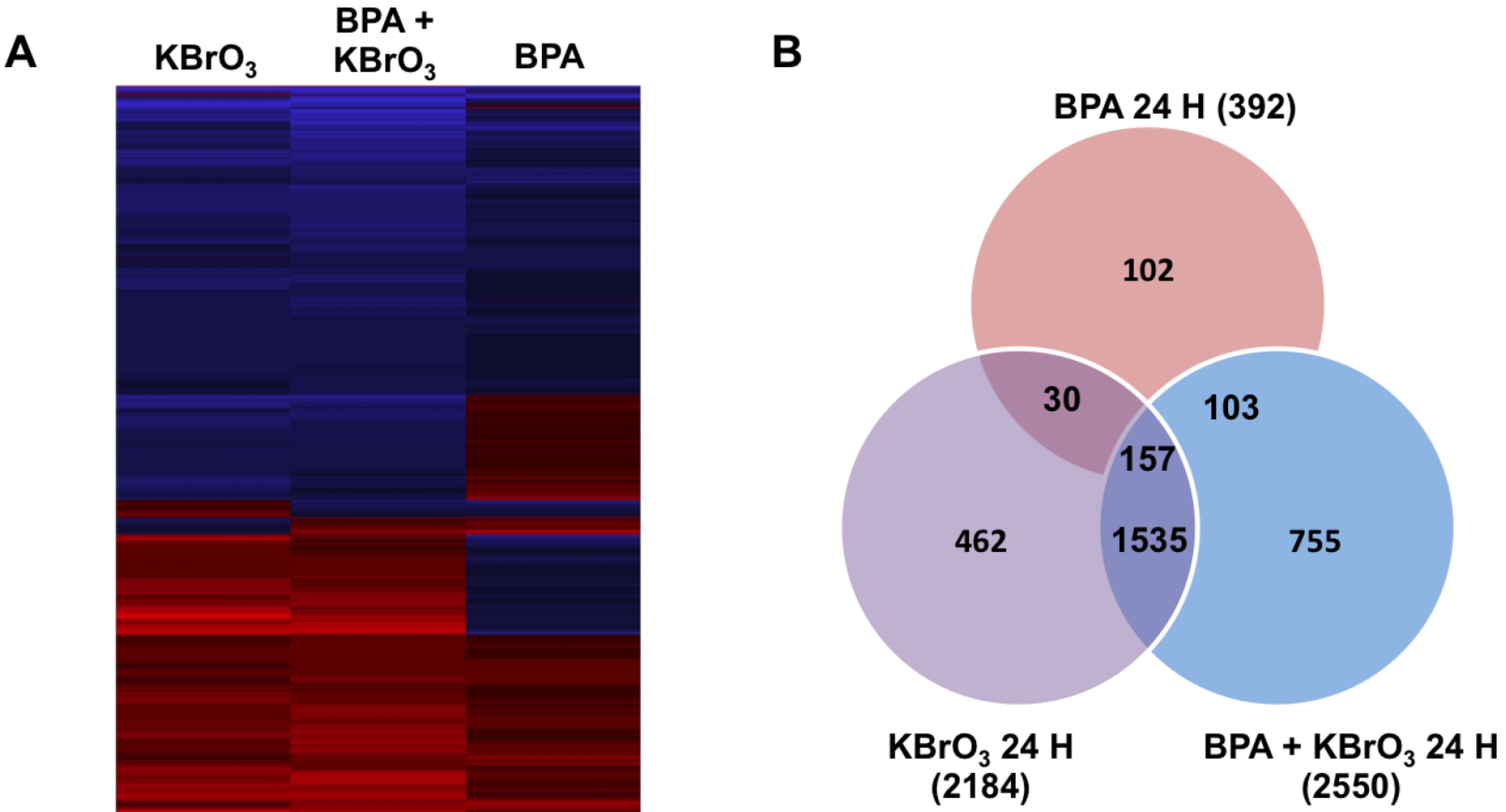
A
KBrO3
BPA + KBrO3
BPA
Minimum
Maximum
Fold Change
-5.00
0.00
5.00
B
BPA 24 H (392)
102
30
103
157
462
1535
755
KBrO3 24 H (2184)
BPA + KBrO3 24 H (2550)

Figure 4.

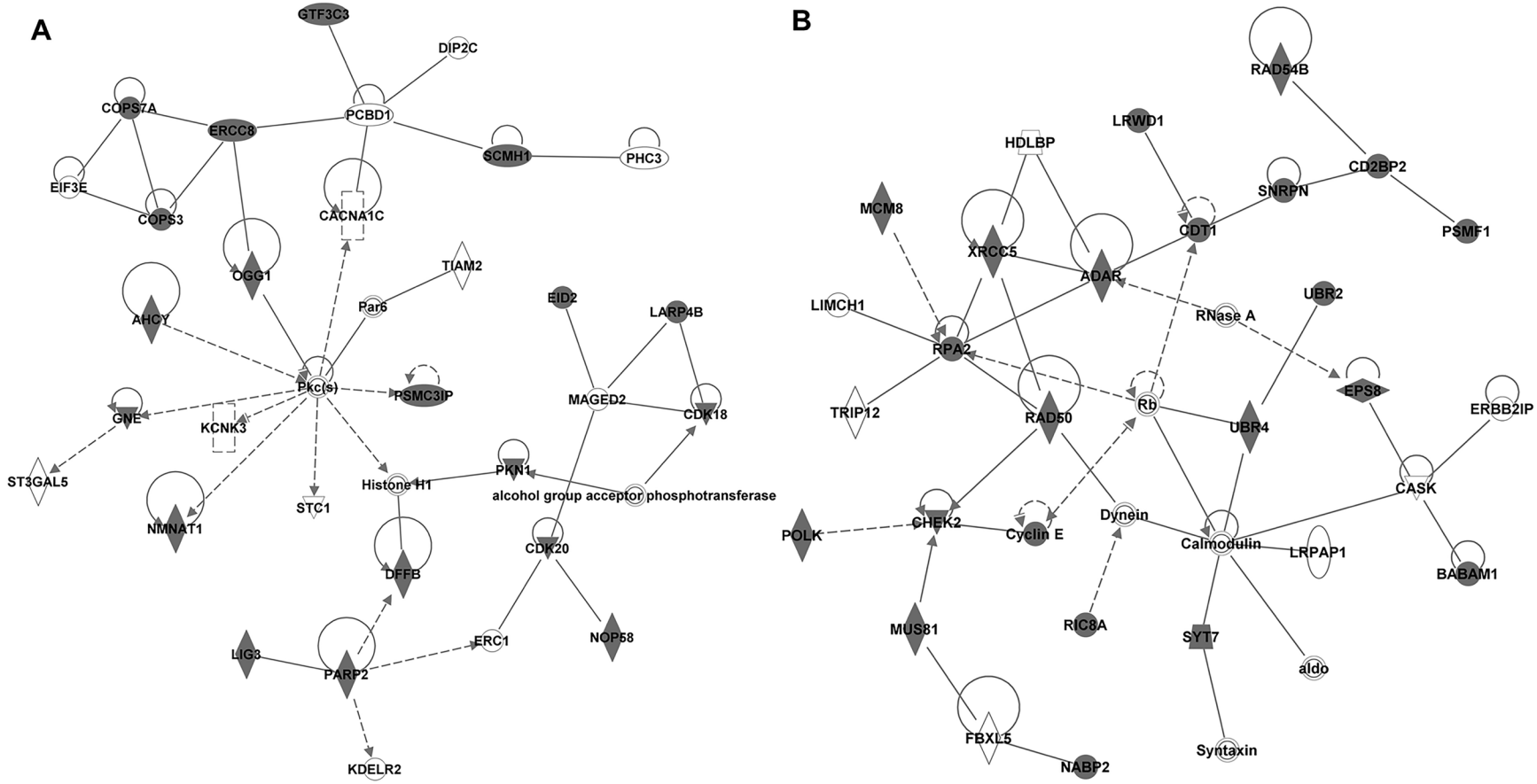
A
GTF3C3
DIP2C
COPS7A
ERCC8
PCBD1
SCMH1
PHC3
EIF3E
COPS3
CACNA1C
OGG1
TIAM2
AHCY
Par6
EID2
LARP4B
Pkc(s)
PSMC3IP
MAGED2
CDK18
GNE
KCNK3
ST3GAL5
Histone H1
PKN1
alcohol group acceptor phosphotransferase
STC1
NMNAT1
CDK20
DFFB
LIG3
PARP2
ERC1
NOP58
KDELR2
B
RAD54B
LRWD1
HDLBP
CD2BP2
SNRPN
MCM8
CDT1
PSMF1
XRCC5
ADAR
UBR2
LIMCH1
RNase A
RPA2
EPS8
TRIP12
RAD50
Rb
UBR4
ERBB2IP
CASK
POLK
CHEK2
Cyclin E
Dynein
Calmodulin
LRPAP1
BABAM1
MUS81
RIC8A
SYT7
aldo
FBXL5
NABP2
Syntaxin

Figure 5.

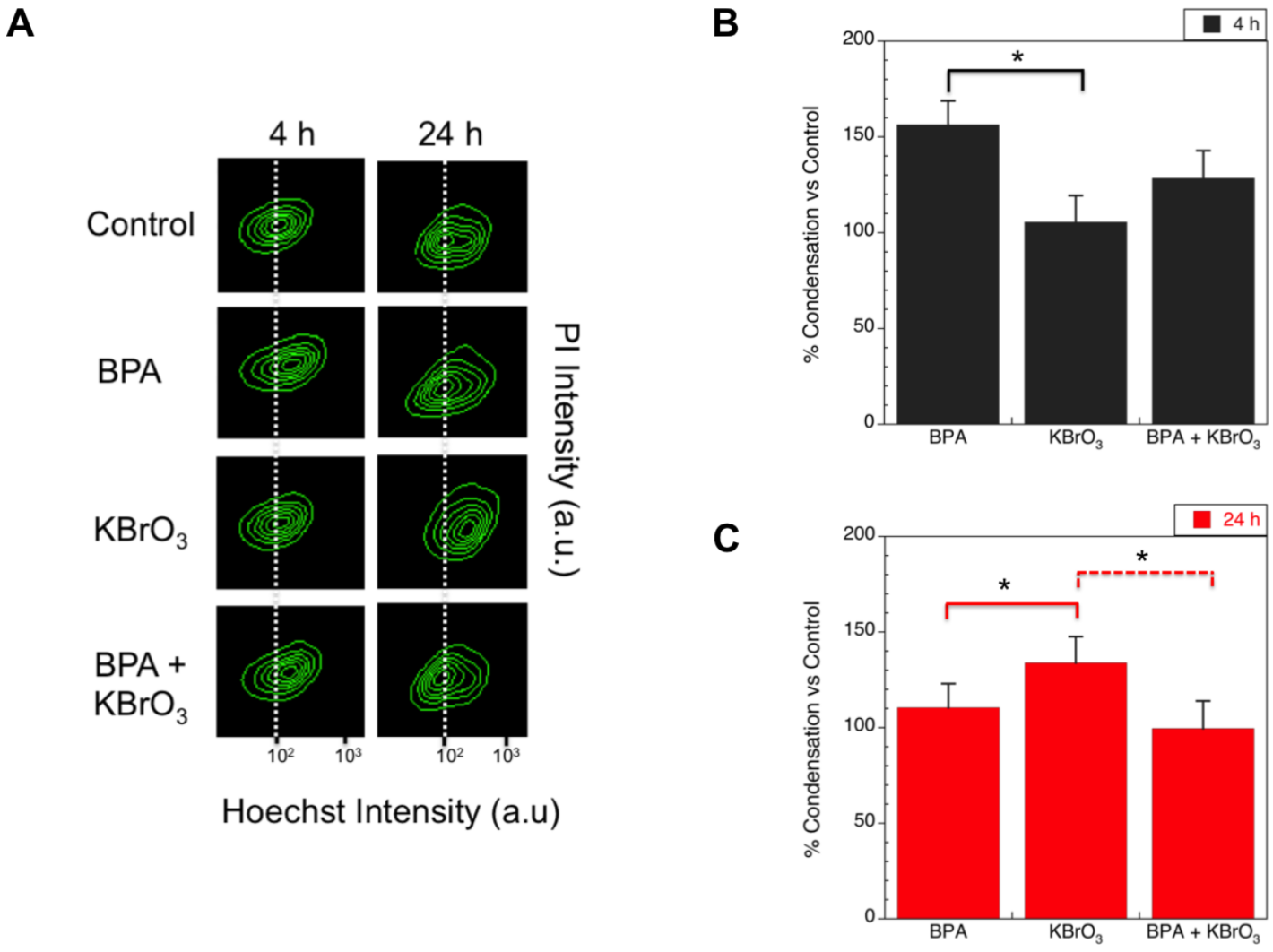
A
4 h
24 h
Control
BPA
KBrO3
BPA + KBrO3
PI Intensity (a.u.)
10²
10³
10²
10³
Hoechst Intensity (a.u)
B
4 h
% Condensation vs Control
200
150
100
50
0
*
BPA
KBrO3
BPA + KBrO3
C
24 h
% Condensation vs Control
200
150
100
50
0
*
*
BPA
KBrO3
BPA + KBrO3

Figure 6.

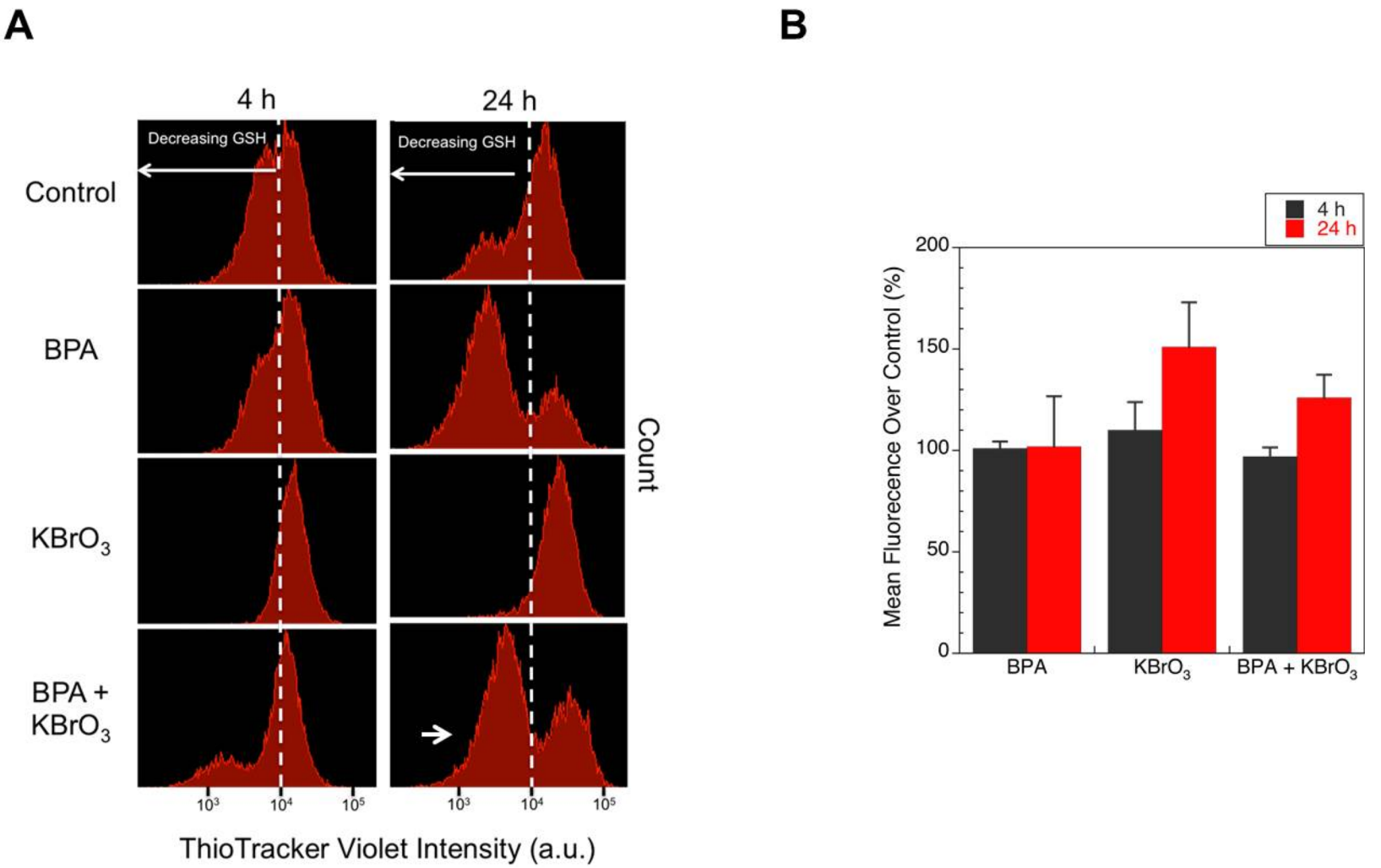
A
4 h
24 h
Decreasing GSH
Decreasing GSH
Control
BPA
KBrO3
BPA + KBrO3
Count
10^3
10^4
10^5
ThioTracker Violet Intensity (a.u.)
B
4 h
24 h
Mean Fluorecence Over Control (%)
200
150
100
50
0
BPA
KBrO3
BPA + KBrO3

Figure 7.

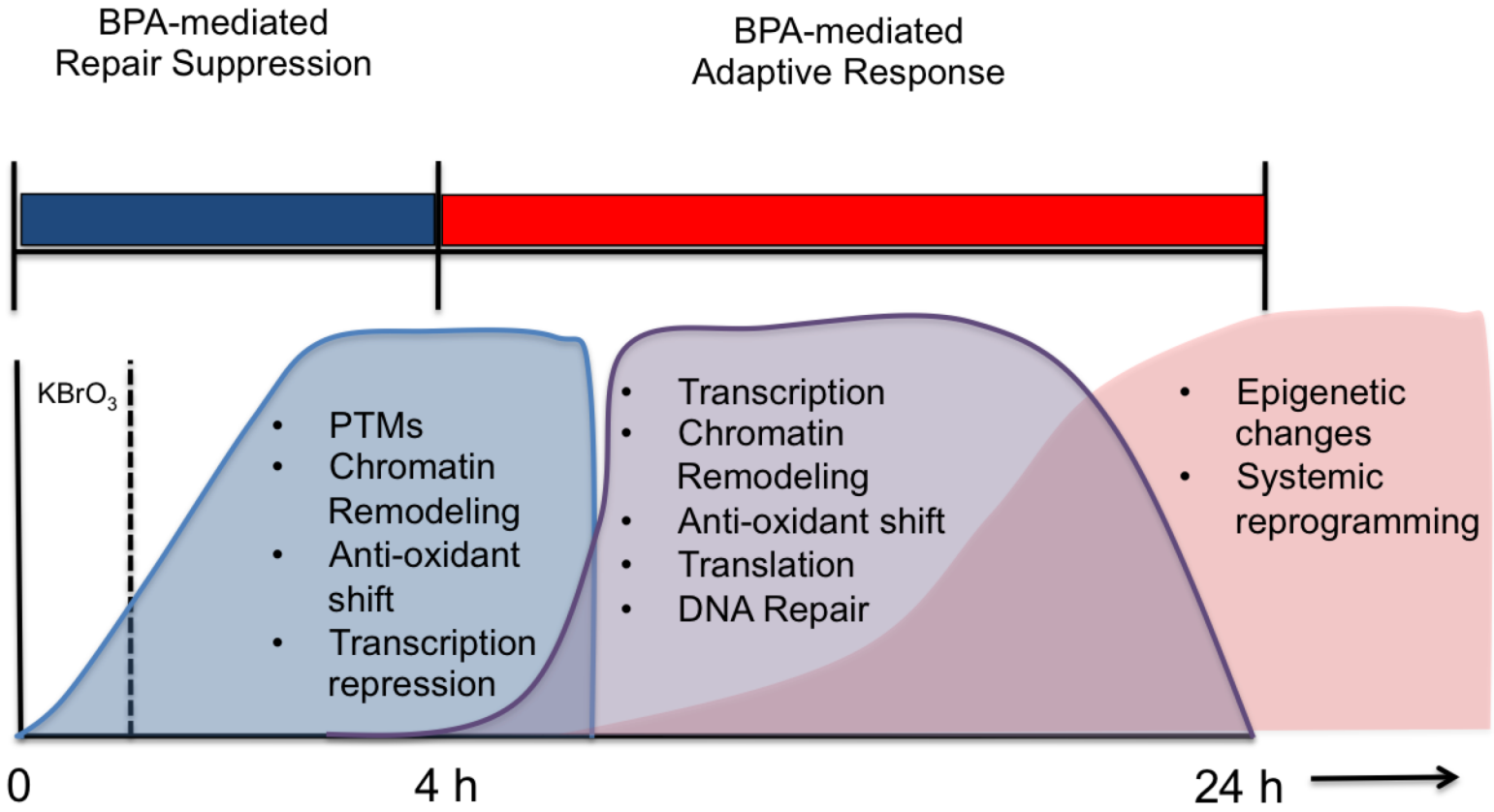
BPA-mediated
Repair Suppression
BPA-mediated
Adaptive Response
KBrO3
• PTMs
• Chromatin Remodeling
• Anti-oxidant shift
• Transcription repression
• Transcription
• Chromatin Remodeling
• Anti-oxidant shift
• Translation
• DNA Repair
• Epigenetic changes
• Systemic reprogramming
0
4 h
24 h